Journal of Materials Chemistry A

ROYAL SOCIETY OF CHEMISTRY

PAPER

View Article Online
View Journal | View Issue

Cite this: J. Mater. Chem. A, 2023, 11, 18302

Understanding the limits of Li-NMC811 half-cells†

Rory C. McNulty, [ab] Elizabeth Hampson,[a] Lewis N. Cutler,[a] Clare P. Grey, [bc] Wesley M. Dose ‡[bc] and Lee R. Johnson *[ab]

Received 15th February 2023
Accepted 2nd August 2023

DOI: 10.1039/d3ta00912b

rsc.li/materials-a

As we push the boundaries of state-of-the-art lithium-ion intercalation materials, such as nickel-rich chemistries, the ability to isolate and understand specific degradation and performance limitations is becoming increasingly important. Half-cells, wherein lithium metal is employed as a dual counter and reference electrode, are commonly used in industry and academia for this purpose. However, the high reactivity of lithium metal drives premature electrolyte degradation and limits cell lifetime, bringing into question the reliability and validity of this cell configuration. Here we explore the limitations of half-cell studies of $LiNi_{0.8}Mn_{0.1}Co_{0.1}O_2$ (NMC811) electrodes with commercially relevant loading. We identify the failure mechanism of this cell configuration through a combination of electrochemical, chemical, and spectroscopic techniques and show that the Li has a direct detrimental impact on the NMC811 chemistry. Our measurements show that vinylene carbonate is critical for these half-cell studies and underpins the cycle limits. Furthermore, we demonstrate the use of $Li_4Ti_5O_{12}$ (LTO) as an alternative counter electrode for understanding the performance of NMC positive electrode materials, due to its high coulombic efficiency and low reactivity with the organic carbonates routinely employed in lithium-ion battery cell chemistries. These data confirm that NMC811 electrodes can tolerate high voltages (stressed) conditions and that cell failure is mainly a result of crossover effects.

Introduction

The current state-of-the-art material classes of nickel-rich positive electrodes are now the standard in automotive commercial cells, typically accommodating a nickel-content of 60% or higher in modern electric vehicles (EVs).[1–3] Early automotive positive electrodes combined equal molar proportions of nickel, manganese, and cobalt, creating the NMC111 ($LiNi_{0.33}Mn_{0.33}Co_{0.33}O_2$) chemistry that provides a capacity performance comparable to that of the ubiquitous lithium cobalt oxide (LCO), with significant reduction of raw materials cost.[4–6] The subsequent push towards high-nickel content was driven by the desire to further increase energy density, while simultaneously limiting raw material cost and reducing cobalt content, a mineral often tarnished by its poor environmental, social and governance record.[7,8] The volumetric energy density of subsequent NMC materials, NMC622 (*ca.* 2600 W h L^{-1}) and NMC811 (*ca.* 3600 W h L^{-1}), have made them the standard for current and future automotive applications, with EV cell manufacturers beginning to implement NMC811+ chemistries in their most recent battery packs.[9–11] This marked increase in capacity performance comes at the cost of increased reactivity of the electrode surface, with Ni^{4+} ions that are formed upon high delithiation of these materials reacting aggressively with the electrolyte components to form a highly resistive cathode electrolyte interphase (CEI).[12–14] Furthermore, this electrode–electrolyte interfacial instability results in crosstalk between the positive and negative electrode, where the formation of acidic species, dissolution of Ni, Mn, and Co ions, and crossover of electrolyte degradation products catalyse further interphase and electrolyte degradation that limit the capacity of the cell.[15–21] This detrimental relationship between increasing nickel content, solid electrolyte interphase (SEI) stability, and capacity fade highlights the need to isolate the positive electrode chemistry and its long-term performance.

The use of half-cells – wherein the electrode of interest is paired with a lithium metal counter electrode – is a common approach in industry and academia for isolated electrochemical analysis of positive electrode materials, with the intrinsically stable reference potential and high specific capacity of lithium metal (3860 mA h g^{-1}) providing an effectively infinite reservoir of lithium ions with minimal impact on the electrochemical response.[22–24] However, the high reactivity of lithium metal with organic carbonates brings into question the reliability of the results produced in these cells, with indiscriminate degradation of the electrolyte components resulting in premature cell death

[a]Nottingham Applied Materials and Interfaces Group, School of Chemistry, University of Nottingham, NG7 2TU, UK. E-mail: lee.johnson@nottingham.ac.uk

[b]The Faraday Institution, Quad One, Harwell Science and Innovation Campus, Didcot, OX11 0RA, UK

[c]Department of Chemistry, University of Cambridge, Lensfield Road, Cambridge, CB2 1EW, UK

† Electronic supplementary information (ESI) available. See DOI: https://doi.org/10.1039/d3ta00912b

‡ Current address: School of Chemistry, University of New South Wales, Sydney, NSW, 2052, Australia.

and increased rate of cell failure compared to a full-cell configuration.[25–27] Current industry standard lithium-ion battery electrolyte solutions are composed of a lithium hexafluorophosphate ($LiPF_6$) salt dissolved in a mixture of cyclic and linear carbonates, normally ethylene carbonate (EC) in combination with one or more linear carbonates: diethyl carbonate (DEC), dimethyl carbonate (DMC), and ethyl methyl carbonate (EMC), all of which undergo reductive decomposition on the surface of lithium metal.[28–30] This base electrolyte composition is often supported by the addition of 2–8 wt% additives with the specific purpose of improving the composition and characteristics of the SEI at the negative electrode.[31–34] While the field is aware of these difficulties, the specific limits and implications on resulting data sets in nickel-rich cells, where performance is increasingly dominated by electrode cross-talk, is not well quantified and no accepted alternative is available.

Here we explore the validity of Li-NMC811 half-cell studies using a commercially relevant electrode loading (16.9 mg cm^{-2}, *ca.* 3.19 mA h cm^{-2}) and electrolyte composition at 40 °C. We determine the limitations of cell cycling and identify the failure mechanisms of these cells. Vinylene carbonate (VC) is examined as the electrolyte additive due to its standard use in commercial NMC811 cell.[10] Time-resolved gas chromatography mass spectrometry (GC-MS), nuclear magnetic resonance (NMR) spectroscopy and electrochemical impedance spectroscopy (EIS) are used to understand the rate of additive consumption and electrolyte degradation. We identify key stages and mechanisms of electrolyte degradation in Li-NMC811 half-cells, and gain insight into the critical cell failure mechanisms. The state of electrode health is explored through cell disassembly, extracting the cycled electrodes and then reconstituting them with a fresh counter electrode and electrolyte. Finally, we demonstrate the use of $Li_4Ti_5O_{12}$ (LTO) as a superior counter electrode that overcomes the shortfall of lithium metal. We show that the high chemical and electrochemical stability of LTO to traditional electrolyte solutions make it an ideal partner electrode for the long-term isolated study of the electrochemical performance of high-nickel electrode chemistries and there electrolyte formulations.

Results and discussion

Half-cell cycling and the role of VC

The long-term half-cell cycling performance of NMC811 at 40 °C was studied using LP57 (1 M $LiPF_6$ in EC : EMC 3 : 7 v/v) as the electrolyte, being employed both in its base composition, with no electrolyte additive, and with the addition of 2 wt% VC additive. High loading cells (16.9 mg cm^{-2}, *ca.* 3.19 mA h cm^{-2}) were used to better replicate commercial conditions, which are expected to exacerbate degradation, in contrast to lower loading cells, where important degradation processes may go unobserved. Cycling studies were performed across two operational potential windows: (1) 3.0–4.2 V, referred to as 'standard' conditions, and (2) 3.0–4.4 V, referred to as a 'stressed' condition, wherein the positive electrode is polarised ~0.2 V past the standard upper cut-off voltage (UCV) into a region where NMC degradation, oxygen loss, oxidation of electrolyte solvent and the VC additive, and increased electrode crosstalk is expected.[35–37] This represents a standard electrolyte formulation for this battery chemistry. All cells were initially cycled between 3.0 and 4.2 V at a rate of C/20 for 2 cycles, providing opportunity for CEI and SEI formation prior to the application of more aggressive cycling conditions. Subsequent cycling was performed at a rate of C/2. Fig. 1 shows a typical example of the capacity performance of these cells accompanied by snapshots of the charge and discharge profiles. Fig. 1A–D show the voltage profiles of Li-NMC811 half-cells at cycling intervals of the 1st C/20 cycle and subsequent 5th, 40th, 50th, 60th, and 100th cycles at C/2. When cycled to an UCV of 4.2 V, all cells exhibited cycling profiles consistent with those previously published.[38–40] Upon extension of the UCV to 4.4 V, a further capacity region providing an initial capacity increase of *ca.* 40 mA h g_{NMC}^{-1} is accessed.

When cycling Li-NMC811 half-cells containing 2 wt% VC, an initial discharge capacity of *ca.* 187 mA h g_{NMC}^{-1} is observed during the initial two C/20 SEI formation cycles, Fig. 1E. Upon initiation of C/2 cycling, discharge capacities of 154.9 and 201.5 mA h g_{NMC}^{-1} were observed for the standard (4.2 V UCV) and stressed (4.4 UCV) cells, respectively. Across the first 50 C/2 cycles, both cells show a high coulombic efficiency, with an average of 99.93% and 99.65% for the standard and stressed cells, respectively. This performance is consistent with the reversible capacity expected for NMC811 electrodes, and high degree of reproducibility is found across multiple cells ran under these conditions, Fig. S1 and S2† (ref. 37). After 50 cycles, a deviation in the coulombic efficiency for both the standard and stressed cells is observed. This drop in coulombic efficiency is indicative of a deviation from the desired intercalation/deintercalation reactions and indicates the onset of irreversible side reactions.[41,42] For both the standard and the stressed cells, the coulombic efficiency continues to decline, and rapid capacity fade is observed. It is important to note that additional side reactions simultaneously occur on the lithium metal-electrolyte interface, forming degradation species that can crossover from the Li electrode to the positive electrode where they will be oxidised. These reactions may impact the coulombic efficiency, however, they will not contribute to loss of lithium inventory due to the excess capacity of the lithium metal electrode causing these reactions to go largely undetected in a half-cell configuration.[43] This drop in coulombic efficiency and rapid capacity fade after 50 cycles is not observed in Gr-NMC811 full-cells cycled with the same cell format to an UCV of 4.2 V, where an average coulombic efficiency >99.9% was recorded over the first 100 C/2 cycles, Fig. S3.† However, when Gr-NMC811 cells are cycled to an UCV of 4.4 V, poor coulombic efficiency and onset of capacity fade are observed throughout the entirety of cycling, attributed to increased electrode crosstalk, Fig. S3,† highlighting the importance of half-cell studies to isolate positive electrode performance.[44–46]

Fig. 1F examines the performance of Li-NMC811 half-cells with no VC present in the electrolyte composition, wherein initial C/2 discharge capacities of 148.2 and 195.0 mA h g_{NMC}^{-1}

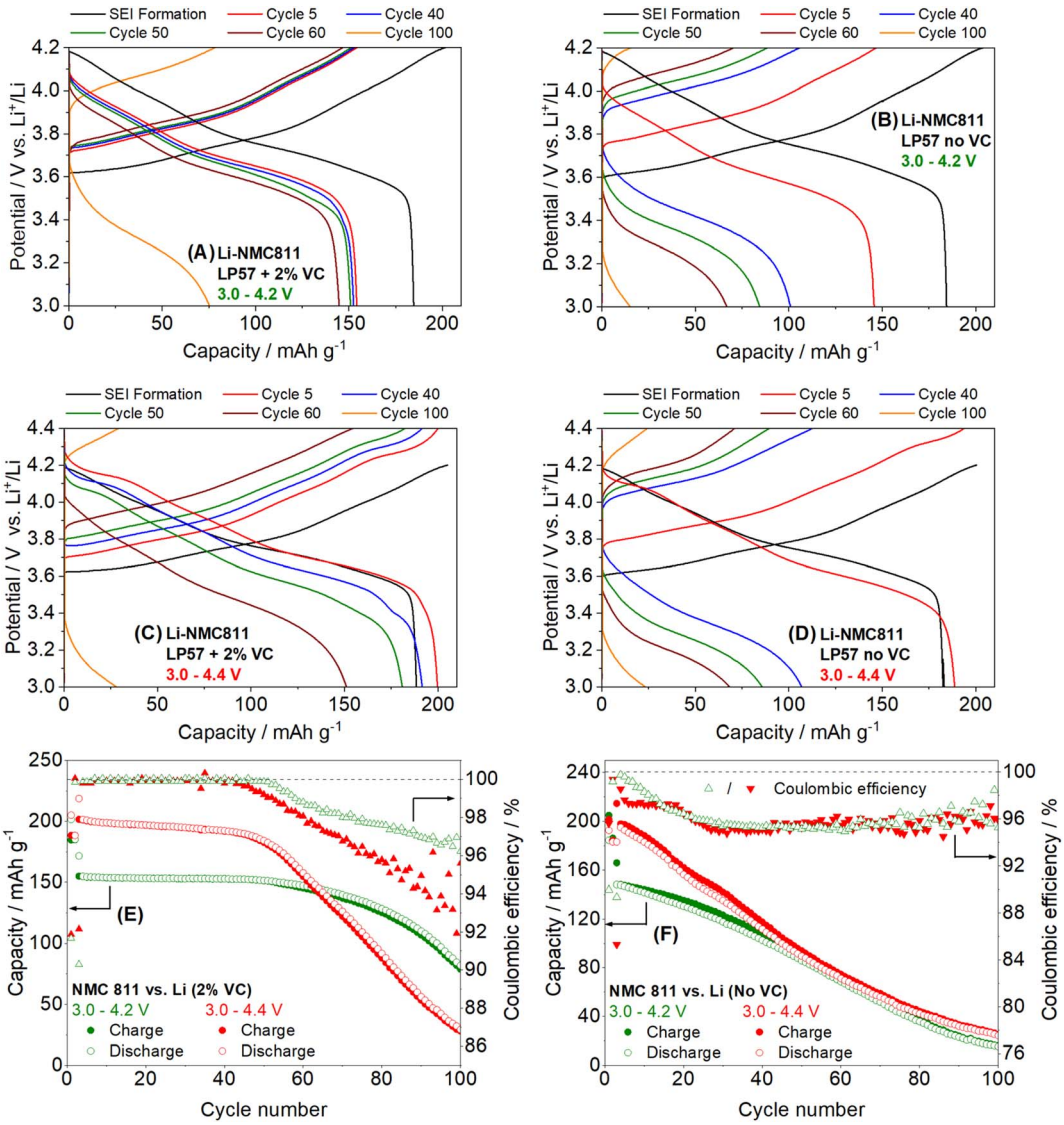

Fig. 1 Comparison of the cycling performance of Li-NMC811 half-cells cycled at 40 °C with an LP57 electrolyte (1 M $LiPF_6$ in EC : EMC 3 : 7 v/v) with and without VC under standard (3.0–4.2 V *vs.* Li^+/Li, green) and stressed (3.0–4.4 V *vs.* Li^+/Li, red) conditions (A–D). Charge and discharge profiles of the initial C/20 SEI formation cycle and the subsequent 5th, 40th, 50th, 60th and 100th cycles carried out at C/2 (E and F). Charge and discharge capacities (circles) and cycle coulombic efficiency (triangles) of the first 100 cycles of (E) with 2 wt% VC additive, and (F) with no additive.

were observed for the standard and stressed cells respectively, comparable to those with VC present. However, the coulombic efficiency of these cells was immediately poor, and no capacity stabilisation is observed. The average coulombic efficiency over the first 50 cycles was 96.3% and 96.0% for the standard and stressed cells, respectively. We note that the cell format, rate and UCV will alter the failure rate. However, measurements in a coin cell format also show a similar effect confirming it as a general problem (Fig. S4†). This data confirms that VC plays a critical role in supporting capacity retention in cells containing lithium metal. Moreover, even when VC is present, the performance deviates from that expected for Gr-NMC811 full-cells after only 50 cycles, bringing into question the validity of lithium metal as a suitable counter electrode in these electrolyte compositions, Fig. S3.†

Electrolyte degradation and the fate of VC

To understand the role that VC plays in delaying the failure of Li-NMC811 cells, GC-MS and NMR spectroscopy were employed to periodically track the consumption of electrolyte species and the resultant formation of degradation products. Fig. 2A shows the GC-MS chromatograms of the extracted electrolyte solution from a cell after 50 and 100 cycles at C/2 to UCVs of both 4.2 and 4.4 V. Electrolyte solution was also extracted from cells rested at OCV for 80 h, the time taken for formation cycling, and analysed as a control. Retention time windows for the organic electrolyte species (EC, EMC, VC) and the most prominent electrolyte degradation species (DEC) are highlighted, with peak assignments confirmed by MS, Fig. S5.† Fig. 2B explores the formation of DEC, commonly reported in literature alongside DMC as the

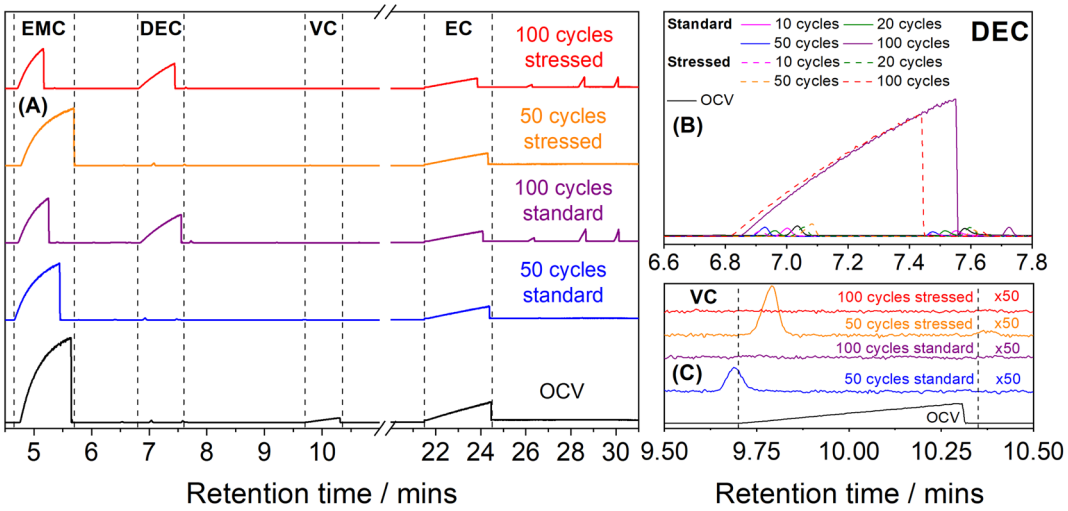

Fig. 2 Analysis of the composition of post-cycled electrolyte solution from Li-NMC811 half-cells by gas chromatography mass spectrometry (GC-MS). Cell contained LP57 electrolyte (1 M $LiPF_6$ in EC : EMC 3 : 7 v/v) with 2 wt% VC additive and were cycled at 40 °C under standard (3.0–4.2 V *vs.* Li^+/Li) or stressed (3.0–4.4 V *vs.* Li^+/Li) conditions. GC-MS traces show (A) full measurement retention window with identified primary peak windows. (B) Retention time window for the DEC region, showing no significant DEC peak until the 100-cycle analysis under both standard and stressed conditions. (C) Retention time window for the VC region, showing the count intensity after an 80 h OCV period (black), 50 cycles (blue) and 100 cycles (purple) under standard cycling conditions, and 50 cycles (orange) and 100 cycles (red) under stressed conditions.

product of the transesterification of EMC through reaction at the negative electrode.[26,47–49] DEC is a common electrolyte solvent used in lithium-ion battery cell chemistries and is not intrinsically detrimental to cell performance,[50,51] but here DEC formation is used as an indicator of the onset of broader electrolyte degradation. After 50 cycles no significant DEC peak is observed, signalling limited electrolyte degradation up to this point and consistent with the stable cycling of these cells, Fig. 2B.[26,47–49] Close inspection of the chromatograms of the extracted electrolyte after 50 cycles reveal that VC is still present in both standard and stressed cells, albeit in low concentration, Fig. 2C. The area of these peaks is <1% of the original VC peak intensity, suggesting that VC will be totally consumed shortly after this observation point. After 100 cycles VC is completely gone, and the area of the DEC peak is now comparable to that of the EMC peak, indicating that significant trans-esterification of EMC takes place within this 50–100 cycle window when no VC remains.

The NMR spectra of the extracted electrolytes are in good agreement with the observations made through analysis of the GC-MS chromatograms, Fig. 3A. The characteristic peak for VC is labelled in the NMR spectrum of the cell rested at OCV for 80 h, with the remaining major peaks in these spectra being characteristic of EC and EMC. Fig. 3B and C examine the VC region of the NMR spectra in greater depth where, although close to the limit of detection of this analytical technique, VC can be identified as still present in the extracted electrolyte solution after 50 cycles. Furthermore, Fig. 3B shows that after 50 cycles the quartet peak characteristic of EMC remains well resolved, indicating no significant quantity of DEC has been formed. After 100 cycles, however, no VC is detected in the NMR spectra and overlapping quartet peaks of both EMC and DEC are observed. The formation of DEC is accompanied by additional peaks in both the GC-MS chromatograms and the NMR spectra, Fig. S6,† indicating a correlation between VC consumption, DEC observation, and the onset of bulk electrolyte degradation. This observation is further reinforced by the immediate observation of DEC formation in the cell cycled with no VC additive, Fig. S7.† The good agreement between the GC-MS and NMR data demonstrates that VC is preferentially degraded on the surface of the lithium metal electrode which mitigates bulk electrolyte degradation resulting in reproducible capacity performance of Li-based half-cell studies when cycle number is limited. Its consumption shortly after 50 cycles and coincident onset of EMC transesterification signifies a relationship between the presence of VC and bulk electrolyte stability.

Identifying the failure mechanism of half-cells based on lithium metal

To understand the origin of the cell failure, electrodes were cycled in cells with VC containing electrolyte under standard conditions for 100 cycles, before being reconstituted – disassembled to remove the cycled electrodes, which are then reassembled in separate cells containing fresh electrolyte and a pristine partner electrode. The full procedure can be found in the ESI† and is validated by disassembling and reassembling cells after 10 cycles, which retain their performance, Fig. S8.† Replenishing the electrolyte acts to simultaneously dilute any remaining contaminants in the cell and re-introduce VC to the system, which can in principle protect the electrolyte solution from further degradation at the surface of the lithium metal electrode. A pristine counter electrode acts to minimise the contribution of the partner electrode to the cell performance, thus elucidating the health of each cycled electrode. Fig. 4 shows the capacity performance and voltage profiles for the first

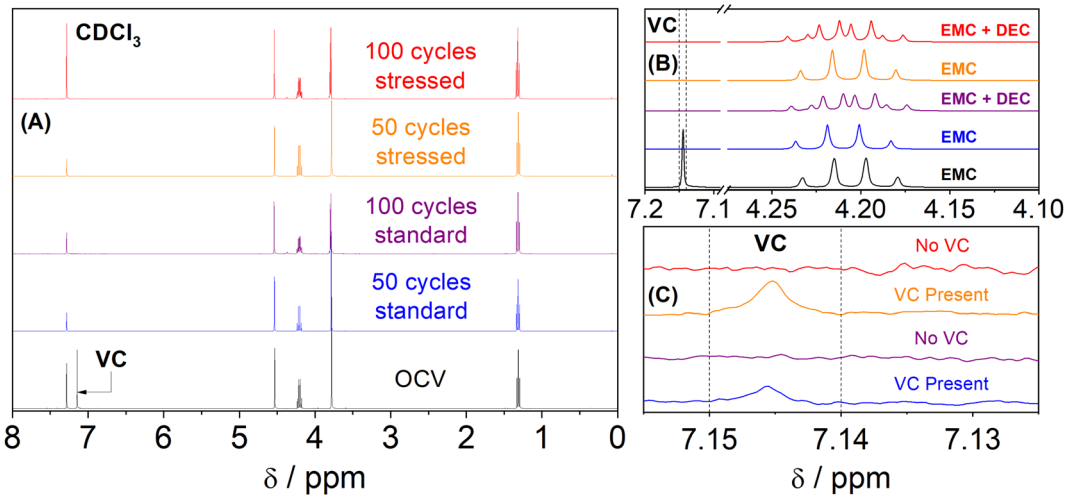

Fig. 3 Analysis of the composition of post-cycled electrolyte solution from Li-NMC811 half-cells by nuclear magnetic resonance spectroscopy. Cell contained LP57 electrolyte (1 M $LiPF_6$ in EC : EMC 3 : 7 v/v) with 2 wt% VC additive and were cycled at 40 °C under standard (3.0–4.2 V *vs.* Li^+/Li) or stressed (3.0–4.4 V *vs.* Li^+/Li) conditions. NMR spectra show (A) full measurement window of interest highlighting the chemical shift of the deuterated solvent ($CDCl_3$) and VC. (B) Chemical shift window for observation of the VC singlet peak and the EMC and DEC quartet peaks, showing no significant DEC peaks until the 100-cycle analysis under both standard and stressed conditions. (C) Enlarged chemical shift window for the VC region, showing small quantities of VC being present after 50 cycles, but no VC remaining in the electrolyte by the 100-cycle point.

two C/20 formation cycles and subsequent C/2 cycle of a pristine cell compared to those for the reconstituted cells. Upon initial C/20 cycling, the NMC811 from cells cycled under standard conditions regained the voltage plateau features that are characteristic of this material, with almost complete capacity recovery (166.6 mA h g_{NMC}^{-1}), Fig. 4A and B. The cycled NMC811 electrode is capable of reversibly intercalating almost the same quantity (89%) of lithium ions as the pristine electrode, demonstrating that the bulk internal structure is largely intact. However, when the rate was increased to C/2, a large drop in the discharge capacity of the cycled NMC811 electrode to 36.9 mA h g_{NMC}^{-1} was observed, Fig. 4A and B, signifying a high impedance. We expect loss of electrolyte volume to be a factor in half-cell failure, but note that during disassembly the cells were not dry and that when replenishing the electrolyte the original performance of these cells does not return. Thus, we suggest electrolyte volume loss is not the major factor impacting performance. The NMC811 from cells cycled to an UCV of 4.4 V before reconstitution showed the same trend, although at C/20 the capacity recovery was less pronounced, and no capacity could be extracted from the electrode upon initiation of C/2 cycling demonstrating higher impedance as a result of a more stressful cycling procedure, Fig. 4A and B. A similar capacity–current relationship is observed for the cell containing the cycled lithium electrode, with cells cycled to an UCV of 4.2 V recording an initial C/20 capacity and a C/2 capacity of 178.7 and 96.0 mA h g_{NMC}^{-1}, respectively, Fig. 4C and D. The cycled lithium metal from cells cycled to an UCV of 4.4 V showed similar C/20 capacity (170.0 mA h g_{NMC}^{-1}) and an increased C/2 capacity (141.2 mA h g_{NMC}^{-1}). The high capacity at C/2 is likely the result of the UCV for C/2 cycling being set at 4.4 V, Fig. 4C and D. This data shows that neither the NMC811 electrode nor the lithium metal electrode are exclusively responsible for the failure of these cells and that both the increased impedance of the cycled NMC811 electrode and degradation of the lithium metal electrode as a result of repeated lithium plating and stripping contribute to the observed capacity loss.

To understand the origin of the impedance of NMC811 electrodes and how it develops as a function of cycle number, EIS was employed in a three-electrode configuration to isolate the positive electrode response, Fig. 5. The impedance response after initial C/20 cycling reveals two distinct semi-circles both with and without VC present, attributed to lithium diffusion through the CEI film (higher frequency, R_{CEI}) and the charge transfer resistance (medium frequency, R_{ct}), Fig. 5A and B.[52] In both cases the RC constants suggest an interfacial process. The uptick observed at low frequencies is attributed to a Warburg impedance (W). The CEI resistance as a function of cycle number was obtained by fitting the data using the equivalent circuit diagram shown in Fig. S9,† 5C and D. For cells containing VC, the CEI film resistance and charge-transfer resistance remained reasonably stable for 50 cycles, Fig. 5C, consistent with the stable cycling capacity shown in Fig. 1. After 50 cycles, when VC is effectively consumed, the CEI resistance in the cell cycled to an UCV of 4.2 V increased from *ca.* 96 to 127 Ω cm^2. In the absence of VC this increase in CEI resistance is observed immediately upon cycling, Fig. 5D. Pushing the UCV to 4.4 V resulted in earlier onsets and greater magnitude of resistance growth, but the overall trends remain. The observed increase in charge transfer resistance when cycling NMC cells above 4.2 V is well documented.[53–55] These results are in line with the cycling data and post-cycling analysis discussed previously, with high CEI film resistance correlating with failure in Li-NMC811 half-cells. To understand the difference in CEI composition under various conditions, X-ray photoelectron spectroscopy (XPS) was performed on NMC811 electrodes after

cycling with and without VC. Spectra of a NMC811 electrode placed in a half-cell at OCV for 80 h (Fig. S10a, d and g†) contained large peaks in the C 1s and F 1s region, consistent with the fluorinated binder material, and peaks in the O 1s region, consistent with the NMC811 electrode. This indicates that no significant CEI forms during OCV. When the electrode was cycled for 2 C/2 formation cycles and 20 subsequent C/2 cycles with no VC additive, none of the peaks representative of the binder or metal oxygen bonds could be observed and significant new organic C–O_x peaks arise, indicating that the CEI mainly consists of organic degradation products and that this is sufficiently thick that the signal from the underlying electrode is blocked (Fig. S10b, e and h†). Where a cell was cycled under the same procedure, but this time with the inclusion of 2 wt% VC, an organic CEI is again seen but the intensity of the peaks is lower, and contributions from the binder remain in the C 1s spectrum (Fig. S10c†), indicating a thinner CEI. Furthermore, a new sp^2 hybridised carbon peak is also observed, which is consistent with a number of organic degradation products.[56,57] In both cases, a strong metal fluorine peak in the F 1s spectra indicates that significant quantities of Li–F have also formed as part of the CEI (Fig. S10h and i†).

Taking our data as a whole, we propose that the preferential degradation of VC at the surface of lithium metal limits electrolyte degradation on both electrodes and enables stable cycling. However, when VC is removed, either directly or through reduction, new electrolyte degradation products are formed at lithium which induce parasitic reactions at the NMC811 electrode and form a resistive CEI. Replenishing VC in the electrolyte after cycling does not lead to a lowering of the impedance or recovery of the capacity (at C/2), indicating that the electrolyte–electrode interfaces of both the NMC811 and lithium electrodes are the issue rather than the composition/properties of the electrolyte.

Lithium titanium oxide as an impartial counter electrode

The findings presented here clearly show that, although the use of lithium metal can in principle eliminate loss of Li^+ inventory as an ageing mechanism, it is an unsuitable candidate for examining the performance of prospective intercalation chemistries beyond early stage cycling due to continued reaction with the electrolyte solution. $Li_4Ti_5O_{12}$ (LTO) negative electrodes have a high operational voltage (1.55 V *vs.* Li^+/Li), do not need to be delithiated prior to use as

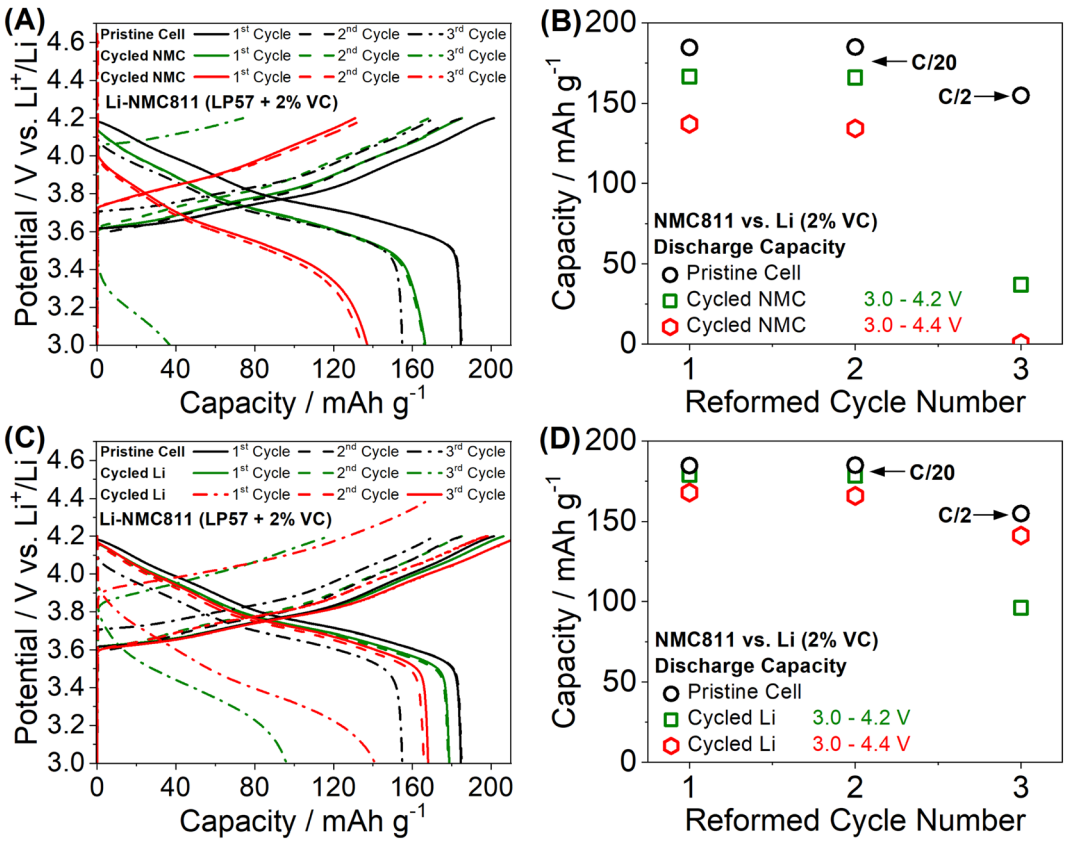

Fig. 4 Comparison of the (A and C) voltage profiles and (B and D) charge and discharge capacities (circles, squares, hexagons) of a pristine Li-NMC811 cell (black, circles) *versus* cells containing (A and B) cycled NMC811 with pristine lithium, and (C and D) pristine NMC811 with cycled Li extracted from the cycled Li-NMC811 half-cells. Cells contained an LP57 electrolyte (1 M $LiPF_6$ in EC : EMC 3 : 7 v/v) with 2 wt% VC additive and were first cycled for 100 cycles under either standard (3.0–4.2 V *vs.* Li^+/Li, green) or stressed (3.0–4.4 V *vs.* Li^+/Li, red) conditions at 40 °C. They were then disassembled and reassembled, pairing both the cycled NMC and cycled Li against pristine (fresh) counter electrodes. The first 2 C/20 formation cycles and first subsequent C/2 cycle of these cells are shown.

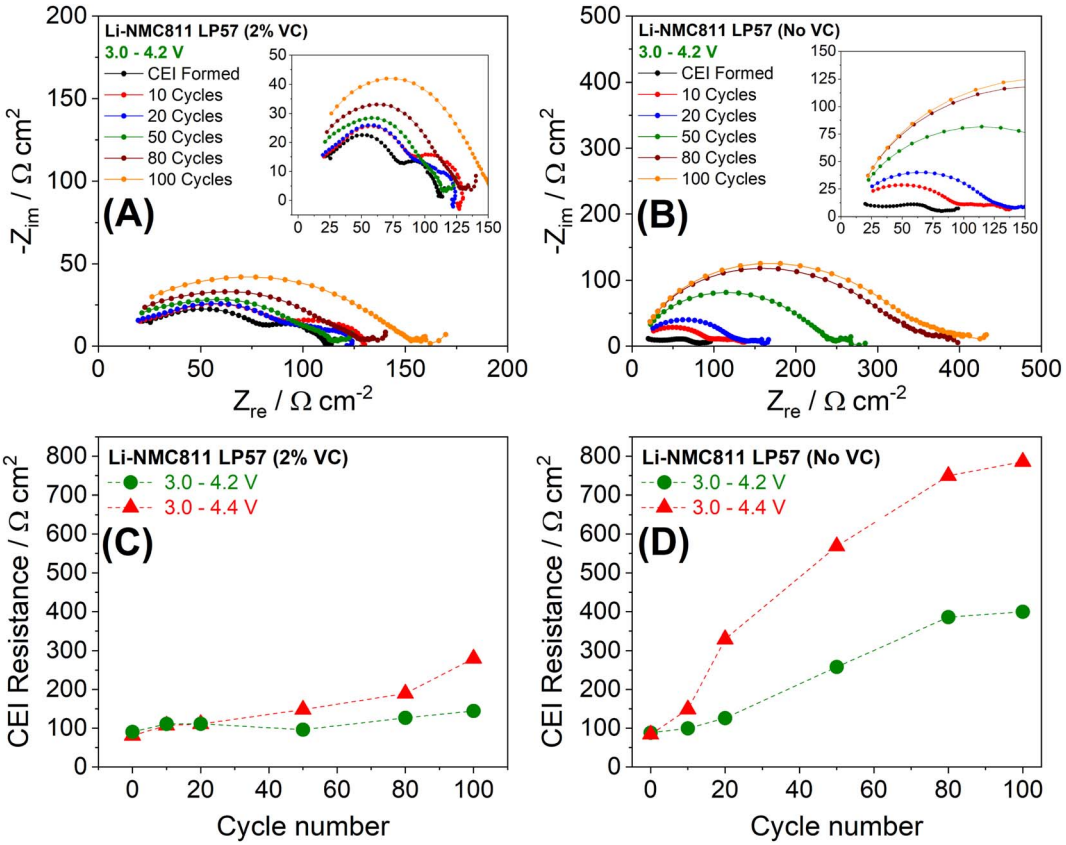

Fig. 5 Comparison of the growth of the resistance of the CEI as a function of cycle number for Li-NMC811 half-cells cycled at 40 °C containing an LP57 electrolyte (1 M $LiPF_6$ in EC : EMC 3 : 7 v/v) both (A and C) with a 2 wt% VC additive and (B and D) with no additive under standard (3.0–4.2 V *vs.* Li^+/Li, green) and stressed (3.0–4.4 V *vs.* Li^+/Li, red) conditions. These measurements were collected in a 3-electrode set up to isolate the impedance response of the NMC electrode at a potential of 3.6 V *vs.* Li^+/Li.

a negative electrode due to intercalation of Li^+ at 1.55 V *vs.* Li/Li^+, and low reactivity with electrolyte components,[58,59] providing an ideal candidate for the isolation of the performance of the prospective positive electrode materials, although lacking the ability of lithium metal to eliminate loss of Li^+ inventory. Although previous reports have indicated that residual water in the electrolyte can reduce on the surface of LTO electrodes to produce hydrogen gas and hydroxide ions that can facilitate additional gassing degradation reactions, adequate measures to limit water intrusion during cell assembly and choice of appropriate cell format mitigate these effects.[60–62] To determine the suitability of LTO as a counter electrode, high loading LTO electrodes (25 mg cm^{-2}, *ca.* 3.7 mA h cm^{-2}), chosen to ensure sufficient counter electrode capacity ($n : p = 1.16 : 1$), were paired against the high loading NMC electrodes (16.9 mg cm^{-2}, *ca.* 3.19 mA h cm^{-2}) used throughout this study. Fig. 6 examines the performance of these cells cycled for 300 cycles under both standard and stressed conditions with no VC additive alongside the GC-MS chromatogram of the electrolytes extracted from these cells. Due to the extremely high loading of the LTO electrodes, rate performance was assessed to determine a charge rate that provided a similar initial capacity to the Li-NMC811 cells, Fig. S11,† with C/5 found to be optimal. Initial C/5 discharge capacities of 167.7 and 201.8 mA h g_{NMC}^{-1} were observed for the standard and stressed cells, respectively, consistent with Li-NMC811 half-cells. For both LTO-NMC811 cells cycled to an UCV of 4.2 V and 4.4 V, coulombic efficiency remained high (>99.6%) over the first 300 cycles, demonstrating that LTO is better able to serve as a non-reactive counter electrode than either lithium metal or graphite, Fig. 6A. Indeed, the stressed cell had a higher capacity performance than both the NMC811 half-cell and full-cell (graphite-based) configurations during extended cycling, Fig. S12,† suggesting that neither of the latter are free of degradation and confirming that crosstalk and parasitic side reactions are largely to blame for NMC811 capacity fade. To confirm the suitability of the LTO electrode as a benign counter electrode, electrolyte degradation was examined through *ex situ* GC-MS analysis of the cycled electrolyte, which showed little degradation of the electrolyte components after >300 cycles, even without the VC additive, Fig. 6B. The only significant additional peak observed in the GC-MS chromatogram was due to the transesterification of EMC to DEC, albeit in much lower concentrations than in the Li-NMC811 half-cells. These data confirm the ability of the LTO counter electrode to portray long-term positive electrode capacity performance more accurately. The use of LTO can introduce additional steps, such as careful cell balancing, but

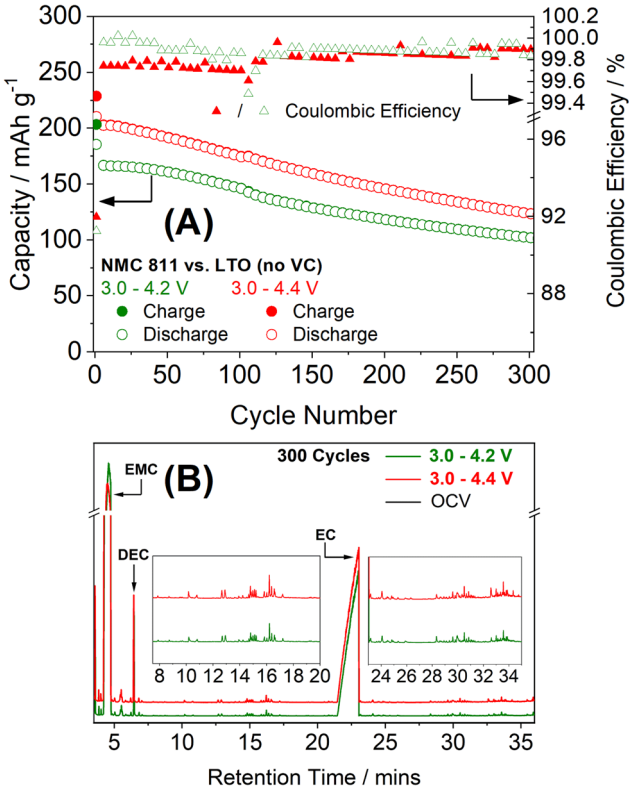

Fig. 6 Comparison of (A) the charge and discharge capacities (circles) and cycle coulombic efficiency (triangles) of the first 300 cycles of LTO-NMC811 cells cycled at 40 °C with an LP57 electrolyte (1 M $LiPF_6$ in EC : EMC 3 : 7 v/v) under standard (3.0–4.2 V *vs.* Li^+/Li, green) and stressed (3.0–4.4 V *vs.* Li^+/Li, red) conditions. (B) GC-MS chromatograms of the electrolyte extracted from these cells after 300 cycles. Potential limits are reported *vs.* Li/Li^+ by addition of 1.55 V to adjust relative to LTO potential.

regardless it could offer a testing ground for electrolyte optimisation targeted at positive electrode stabilisation, without the complexities introduced by traditional full-cell and half-cell formats.

Conclusions

Despite the prevalence of lithium metal half-cells in literature, we have shown that this configuration offers a limited reliable cycle life and that the use of vinylene carbonate as a sacrificial additive is essential. Following a brief period of stability, indiscriminate degradation of the electrolyte solution at the surface of the lithium metal produces parasitic degradation products that crossover the cell and are oxidised at the surface of the positive electrode, resulting in increased interfacial resistance that prematurely limit the capacity and rate performance of the electrode. At C/20, cycled NMC811 electrodes show lithium insertion capacity close to pristine, confirming that cell performance is an artifact of the Li-based half-cell rather than being specific to the intercalation material under consideration. The need to tailor the electrolyte solution to accommodate the lithium metal electrode and the significant degradation precludes informative study of electrolyte additives designed for the positive electrode. LTO is proposed as an alternative counter electrode for the isolated study of positive electrode material performance. LTO-NMC811 cells have a high coulombic efficiency in commercially relevant electrolytes, under both standard and stressed conditions, making them ideal for long-term investigation of prospective intercalation chemistries. Over 300 cycles with no electrolyte additive, LTO-NMC811 cells cycled to an UCV of 4.4 V outperform both Li-NMC811 and Gr-NMC811 cells, confirming that capacity fade in current half- and full-cell formats cycled to high UCVs is not exclusively the result of positive electrode failure, but also a result of increased electrode crosstalk. We propose this cell chemistry will find application in exploration of electrolyte compositions targeted at positive electrode stabilisation without significant complication due to chemical and electrochemical activity of the counter electrode.

Author contributions

RCM, EH, CPG, WMD and LJ contributed to the conception and design of the study. RCM, EH, and LNC performed the experiments. RCM wrote the first draft of the manuscript and all authors contributed to manuscript revisions and read and approved the submitted version. CPG, WMD and LJ supervised the project.

Conflicts of interest

There are no conflicts to declare.

Acknowledgements

LJ, WMD, CPG and RM gratefully acknowledge the support of the Faraday Institution's degradation project (EP/S003053/1 FITG001, FIRG014, FIRG024, FIRG044, EP/S514901/1). LJ and RM gratefully acknowledge support from the University of Nottingham's Propulsion Futures Beacon of Excellence for supporting this research. LJ is grateful to the EPSRC fellowship scheme (EP/S001611/1). The authors are grateful to A. Jansen, S. E. Trask, B. J. Polzin, and A. R. Dunlop at the U.S. Department of Energy's CAMP (Cell Analysis, Modelling, and Prototyping) Facility, Argonne National Laboratory, for producing and supplying the LTO electrodes in this work.

References

1 W. Li, E. M. Erickson and A. Manthiram, High-nickel layered oxide cathodes for lithium-based automotive batteries, *Nat. Energy*, 2020, **5**, 26–34, DOI: 10.1038/s41560-019-0513-0.
2 C. Xu, Q. Dai, L. Gaines, M. Hu, A. Tukker and B. Steubing, Future material demand for automotive lithium-based batteries, *Commun. Mater.*, 2020, **1**, 99, DOI: 10.1038/s43246-020-00095-x.
3 D. Andre, S.-J. Kim, P. Lamp, S. F. Lux, F. Maglia, O. Paschos and B. Stiaszny, Future generations of cathode materials: an

automotive industry perspective, *J. Mater. Chem. A*, 2015, **3**, 6709–6732, DOI: 10.1039/C5TA00361J.

4 A. Masias, J. Marcicki and W. A. Paxton, Opportunities and challenges of lithium ion batteries in automotive applications, *ACS Energy Lett.*, 2021, **6**, 621–630, DOI: 10.1021/acsenergylett.0c02584.

5 F. Duffner, M. Wentker, M. Greenwood and J. Leker, Battery cost modeling: a review and directions for future research, *Renewable Sustainable Energy Rev.*, 2020, **127**, 109872, DOI: 10.1016/j.rser.2020.109872.

6 A. Manthiram, A reflection on lithium-ion battery cathode chemistry, *Nat. Commun.*, 2020, **11**, 1–9, DOI: 10.1038/s41467-020-15355-0.

7 E. A. Olivetti, G. Ceder, G. G. Gaustad and X. Fu, Lithium-ion battery supply chain considerations: analysis of potential bottlenecks in critical metals, *Joule*, 2017, **1**, 229–243, DOI: 10.1016/j.joule.2017.08.019.

8 B. E. Murdock, K. E. Toghill and N. Tapia-Ruiz, A perspective on the sustainability of cathode materials used in lithium-ion batteries, *Adv. Energy Mater.*, 2021, **11**, 2102028, DOI: 10.1002/aenm.202102028.

9 C.-H. Chen, F. B. Planella, K. O'Regan, D. Gastol, W. D. Widanage and E. Kendrick, Development of experimental techniques for parameterization of multi-scale lithium-ion battery models, *J. Electrochem. Soc.*, 2020, **167**, 080534, DOI: 10.1149/1945-7111/ab9050.

10 F. J. Günter and N. Wassiliadis, State of the art of lithium-ion pouch cells in automotive applications: cell teardown and characterization, *J. Electrochem. Soc.*, 2022, **169**, 030515, DOI: 10.1149/1945-7111/ac4e11.

11 G. Kovachev, H. Schröttner, G. Gstrein, L. Aiello, I. Hanzu, H. M. R. Wilkening, A. Foitzik, M. Wellm, W. Sinz and C. Ellersdorfer, Analytical dissection of an automotive li-ion pouch cell, *Batteries*, 2019, **5**, 67, DOI: 10.3390/batteries5040067.

12 T. Li, X.-Z. Yuan, L. Zhang, D. Song, K. Shi and C. Bock, Degradation mechanisms and mitigation strategies of nickel-rich NMC-based lithium-ion batteries, *Electrochem. Energy Rev.*, 2020, **3**, 43–80, DOI: 10.1007/s41918-019-00053-3.

13 W. Liu, P. Oh, X. Liu, M. J. Lee, W. Cho, S. Chae, Y. Kim and J. Cho, Nickel-rich layered lithium transition-metal oxide for high-energy lithium-ion batteries, *Angew. Chem., Int. Ed.*, 2015, **54**, 4440–4457, DOI: 10.1002/anie.201409262.

14 N.-H. Yeh, F.-M. Wang, C. Khotimah, X.-C. Wang, Y.-W. Lin, S.-C. Chang, C.-C. Hsu, Y.-J. Chang, L. Tiong, C.-H. Liu, *et al.*). Controlling Ni^{2+} from the surface to the bulk by a new cathode electrolyte interphase formation on a ni-rich layered cathode in high-safe and high-energy-density lithium-ion batteries, *ACS Appl. Mater. Interfaces*, 2021, **13**, 7355–7369, DOI: 10.1021/acsami.0c22295.

15 Z. Ruff, C. Xu and C. P. Grey, Transition metal dissolution and degradation in NMC811-graphite electrochemical cells, *J. Electrochem. Soc.*, 2021, **168**, 060518, DOI: 10.1149/1945-7111/ac0359.

16 H. Zheng, Q. Sun, G. Liu, X. Song and V. S. Battaglia, Correlation between dissolution behavior and electrochemical cycling performance for $LiNi_{1/3}Co_{1/3}Mn_{1/3}O_2$-based cells, *J. Power Sources*, 2012, **207**, 134–140, DOI: 10.1016/j.jpowsour.2012.01.122.

17 D. R. Gallus, R. Schmitz, R. Wagner, B. Hoffmann, S. Nowak, I. Cekic-Laskovic, R. W. Schmitz and M. Winter, The influence of different conducting salts on the metal dissolution and capacity fading of NCM cathode material, *Electrochim. Acta*, 2014, **134**, 393–398, DOI: 10.1016/j.electacta.2014.04.091.

18 B. L. D. Rinkel, D. S. Hall, I. Temprano and C. P. Grey, Electrolyte oxidation pathways in lithium-ion batteries, *J. Am. Chem. Soc.*, 2020, **142**, 15058–15074, DOI: 10.1021/jacs.0c06363.

19 C. Jayawardana, N. D. Rodrigo, L. Rynearson and B. L. Lucht, Difluorophosphoric acid generation and crossover reactions in $LiNi_xCo_yMn_zO_2$ cathodes operating at high voltage, *J. Electrochem. Soc.*, 2022, **169**, 060509, DOI: 10.1149/1945-7111/ac72c7.

20 J. A. Gilbert, I. A. Shkrob and D. P. Abraham, Transition metal dissolution, ion migration, electrocatalytic reduction and capacity loss in lithium-ion full cells, *J. Electrochem. Soc.*, 2017, **164**, A389–A399, DOI: 10.1149/2.1111702jes.

21 R. Jung, F. Linsenmann, R. Thomas, J. Wandt, S. Solchenbach, F. Maglia, C. Stinner, M. Tromp and H. A. Gasteiger, Nickel, manganese, and cobalt dissolution from Ni-Rich NMC and their effects on NMC622-graphite cells, *J. Electrochem. Soc.*, 2019, **166**, A378–A389, DOI: 10.1149/2.1151902jes.

22 B. Rowden and N. Garcia-Araez, Estimating lithium-ion battery behavior from half-cell data, *Energy Rep*, 2021, **7**, 97–103, DOI: 10.1016/j.egyr.2021.02.048.

23 E. Miele, W. M. Dose, I. Manyakin, M. H. Frosz, Z. Ruff, M. F. L. De Volder, C. P. Grey, J. J. Baumberg and T. G. Euser, Hollow-core optical fibre sensors for operando Raman spectroscopy investigation of Li-ion battery liquid electrolytes, *Nat. Commun.*, 2022, **13**, 1651, DOI: 10.1038/s41467-022-29330-4.

24 M. C. Schulze and N. R. Neale, Half-cell cumulative efficiency forecasts full-cell capacity retention in lithium-ion batteries, *ACS Energy Lett.*, 2021, **6**, 1082–1086, DOI: 10.1021/acsenergylett.1c00173.

25 J. Li, L. E. Downie, L. Ma, W. Qiu and J. R. Dahn, Study of the failure mechanisms of $LiNi_{0.8}Mn_{0.1}Co_{0.1}O_2$ cathode material for lithium ion batteries, *J. Electrochem. Soc.*, 2015, **162**, A1401, DOI: 10.1149/2.1011507jes.

26 F. M. Weber, I. Kohlhaas and E. Figgemeier, Tuning the reactivity of electrolyte solvents on lithium metal by vinylene carbonate, *J. Electrochem. Soc.*, 2020, **167**, 140523, DOI: 10.1149/1945-7111/abc436.

27 G. Zhuang, Y. Chen and P. N. Ross, The reaction of lithium with dimethyl carbonate and diethyl carbonate in ultrahigh vacuum studied by X-ray photoemission spectroscopy, *Langmuir*, 1999, **15**, 1470–1479, DOI: 10.1021/la980454y.

28 M. Armand, P. Axmann, D. Bresser, M. Copley, K. Edström, C. Ekberg, D. Guyomard, B. Lestriez, P. Novák, M. Petranikova, *et al.*). Lithium-ion batteries – current state of the art and anticipated developments, *J. Power*

Sources, 2020, **479**, 228708, DOI: 10.1016/j.jpowsour.2020.228708.

29 S. K. Heiskanen, J. Kim and B. L. Lucht, Generation and evolution of the solid electrolyte interphase of lithium-ion batteries, *Joule*, 2019, **3**, 2322–2333, DOI: 10.1016/j.joule.2019.08.018.

30 J. Xie and Y.-C. Lu, A retrospective on lithium-ion batteries, *Nat. Commun.*, 2020, **11**, 2499, DOI: 10.1038/s41467-020-16259-9.

31 P. G. Kitz, M. J. Lacey, P. Novák and E. J. Berg, Operando investigation of the solid electrolyte interphase mechanical and transport properties formed from vinylene carbonate and fluoroethylene carbonate, *J. Power Sources*, 2020, **477**, 228567, DOI: 10.1016/j.jpowsour.2020.228567.

32 H. Nakai, T. Kubota, A. Kita and A. Kawashima, Investigation of the solid electrolyte interphase formed by fluoroethylene carbonate on Si electrodes, *J. Electrochem. Soc.*, 2011, **158**, A798, DOI: 10.1149/1.3589300.

33 A. M. Haregewoin, A. S. Wotango and B.-J. Hwang, Electrolyte additives for lithium ion battery electrodes: progress and perspectives, *Energy Environ. Sci.*, 2016, **9**, 1955–1988, DOI: 10.1039/C6EE00123H.

34 D. Aurbach, K. Gamolsky, B. Markovsky, Y. Gofer, M. Schmidt and U. Heider, On the use of vinylene carbonate (VC) as an additive to electrolyte solutions for Li-ion batteries, *Electrochim. Acta*, 2002, **47**, 1423–1439, DOI: 10.1016/S0013-4686(01)00858-1.

35 W. M. Dose, C. Xu, C. P. Grey and M. F. L. De Volder, Effect of anode slippage on cathode cutoff potential and degradation mechanisms in Ni-Rich Li-ion batteries, *Cell Rep. Phys. Sci.*, 2020, **1**, 100253, DOI: 10.1016/j.xcrp.2020.100253.

36 J. Li, H. Liu, J. Xia, A. R. Cameron, M. Nie, G. A. Botton and J. R. Dahn, The impact of electrolyte additives and upper cut-off voltage on the formation of a rocksalt surface layer in $LiNi_{0.8}Mn_{0.1}Co_{0.1}O_2$ electrodes, *J. Electrochem. Soc.*, 2017, **164**, A655–A665, DOI: 10.1149/2.0651704jes.

37 R. Jung, M. Metzger, F. Maglia, C. Stinner and H. A. Gasteiger, Oxygen release and its effect on the cycling stability of $LiNi_xMn_yCo_zO_2$ (NMC) cathode materials for li-ion batteries, *J. Electrochem. Soc.*, 2017, **164**, A1361–A1377, DOI: 10.1149/2.0021707jes.

38 H.-J. Noh, S. Youn, C. S. Yoon and Y.-K. Sun, Comparison of the structural and electrochemical properties of layered Li$[Ni_xCo_yMn_z]O_2$ ($x = 1/3$, 0.5, 0.6, 0.7, 0.8 and 0.85) cathode material for lithium-ion batteries, *J. Power Sources*, 2013, **233**, 121–130, DOI: 10.1016/j.jpowsour.2013.01.063.

39 H.-H. Ryu, K.-J. Park, C. S. Yoon and Y.-K. Sun, Capacity fading of Ni-rich $Li[Ni_xCo_yMn_{1-x-y}]O_2$ ($0.6 \leq x \leq 0.95$) cathodes for high-energy-density lithium-ion batteries: bulk or surface degradation?, *Chem. Mater.*, 2018, **30**, 1155–1163, DOI: 10.1021/acs.chemmater.7b05269.

40 K. Märker, P. J. Reeves, C. Xu, K. J. Griffith and C. P. Grey, Evolution of structure and lithium dynamics in $LiNi_{0.8}Mn_{0.1}Co_{0.1}O_2$ (NMC811) cathodes during electrochemical cycling, *Chem. Mater.*, 2019, **31**, 2545–2554, DOI: 10.1021/acs.chemmater.9b00140.

41 A. A. Rulev, A. Frolov, S. Doronin, I. Bezuglov, D. M. Itkis and L. V. Yashina, Revising the pathways of the Li reaction with organic carbonates, *Phys. Chem. Chem. Phys.*, 2020, **22**, 16184–16192, DOI: 10.1039/D0CP02228D.

42 R. Dedryvère, S. Laruelle, S. Grugeon, L. Gireaud, J.-M. Tarascon and D. Gonbeau, XPS identification of the organic and inorganic components of the electrode/electrolyte interface formed on a metallic cathode, *J. Electrochem. Soc.*, 2005, **152**, A689, DOI: 10.1149/1.1861994.

43 J. Xiao, Q. Li, Y. Bi, M. Cai, B. Dunn, T. Glossmann, J. Liu, T. Osaka, R. Sugiura, B. Wu, *et al.*). Understanding and applying coulombic efficiency in lithium metal batteries, *Nat. Energy*, 2020, **5**, 561–568, DOI: 10.1038/s41560-020-0648-z.

44 O. C. Harris, S. E. Lee, C. Lees and M. Tang, Review: mechanisms and consequences of chemical cross-talk in advanced Li-ion batteries, *J. Phys. Energy*, 2020, **2**, 032002, DOI: 10.1088/2515-7655/ab8b68.

45 W. Li, X. Liu, Q. Xie, Y. You, M. Chi and A. Manthiram, Long-term cyclability of NCM-811 at high voltages in lithium-ion batteries: an in-depth diagnostic study, *Chem. Mater.*, 2020, **32**, 7796–7804, DOI: 10.1021/acs.chemmater.0c02398.

46 T. M. M. Heenan, A. Jnawali, M. D. R. Kok, T. G. Tranter, C. Tan, A. Dimitrijevic, R. Jervis, D. J. L. Brett and P. R. Shearing, An advanced microstructural and electrochemical datasheet on 18650 Li-ion batteries with nickel-rich NMC811 cathodes and graphite-silicon anodes, *J. Electrochem. Soc.*, 2020, **167**, 140530, DOI: 10.1149/1945-7111/abc4c1.

47 D. Aurbach, B. Markovsky, A. Shechter, Y. Ein-Eli and H. Cohen, A comparative study of synthetic graphite and Li electrodes in electrolyte solutions based on ethylene carbonate-dimethyl carbonate mixtures, *J. Electrochem. Soc.*, 1996, **143**, 3809–3820, DOI: 10.1149/1.1837300.

48 R. Petibon, L. Rotermund, K. J. Nelson, A. S. Gozdz, J. Xia and J. R. Dahn, Study of electrolyte components in Li ion cells using liquid-liquid extraction and gas chromatography coupled with mass spectrometry, *J. Electrochem. Soc.*, 2014, **161**, A1167–A1172, DOI: 10.1149/2.117406jes.

49 B. Strehle, S. Solchenbach, M. Metzger, K. U. Schwenke and H. A. Gasteiger, The effect of CO_2 on alkyl carbonate transesterification during formation of graphite electrodes in li-ion batteries, *J. Electrochem. Soc.*, 2017, **164**, A2513, DOI: 10.1149/2.1001712jes.

50 E. Quartarone and P. Mustarelli, Review—emerging trends in the design of electrolytes for lithium and post-lithium batteries, *J. Electrochem. Soc.*, 2020, **167**, 050508, DOI: 10.1149/1945-7111/ab63c4.

51 K. Xu, Electrolytes and interphases in Li-ion batteries and beyond, *Chem. Rev.*, 2014, **114**, 11503–11618, DOI: 10.1021/cr500003w.

52 X. Wang, J. Cai, Y. Ren, M. Benamara, X. Zhou, Y. Li, Z. Chen, H. Zhou, X. Xiao, Y. Liu, *et al.*). High-performance $LiNi_{0.8}Mn_{0.1}Co_{0.1}O_2$ cathode by nanoscale lithium sulfide coating *via* atomic layer deposition, *J. Energy Chem.*, 2022, **69**, 531–540, DOI: 10.1016/j.jechem.2022.02.015.

53 W. M. Dose, J. K. Morzy, A. Mahadevegowda, C. Ducati, C. P. Grey and M. F. L. De Volder, The influence of electrochemical cycling protocols on capacity loss in nickel-rich lithium-ion batteries, *J. Mater. Chem. A*, 2021, **9**, 23582–23596, DOI: **10.1039/D1TA06324C**.

54 L. Zhang, C. Zhang, N. Li and W. Tong, Influence of charge cutoff voltage on the cycling behavior of $LiNi_{0.5}Mn_{0.3}Co_{0.2}O_2$ cathode, *J. Electrochem. Soc.*, 2020, **167**, 120509, DOI: **10.1149/1945-7111/abaa17**.

55 V. Charbonneau, A. Lasia and G. Brisard, Impedance studies of Li^+ diffusion in nickel manganese cobalt oxide (NMC) during charge/discharge cycles, *J. Electroanal. Chem.*, 2020, **875**, 113944, DOI: **10.1016/j.jelechem.2020.113944**.

56 W. M. Dose, I. Temprano, J. P. Allen, E. Björklund, C. A. O'Keefe, W. Li, B. L. Mehdi, R. S. Weatherup, M. F. L. De Volder and C. P. Grey, Electrolyte reactivity at the charged Ni-rich cathode interface and degradation in Li-ion batteries, *ACS Appl. Mater. Interfaces*, 2022, **14**, 13206–13222, DOI: **10.1021/acsami.1c22812**.

57 M. Hekmatfar, I. Hasa, R. Eghbal, D. V. Carvalho, A. Moretti and S. Passerini, Effect of electrolyte additives on the $LiNi_{0.5}Mn_{0.3}Co_{0.2}O_2$ surface film formation with lithium and graphite negative electrodes, *Adv. Mater. Interfaces*, 2020, 7, 1901500, DOI: **10.1002/admi.201901500**.

58 W. M. Dose, W. Li, I. Temprano, C. A. O'Keefe, B. L. Mehdi, M. F. L. De Volder and C. P. Grey, Onset potential for electrolyte oxidation and Ni-rich cathode degradation in lithium-ion batteries, *ACS Energy Lett*, 2022, 3524–3530, DOI: **10.1021/acsenergylett.2c01722**.

59 A. Tornheim, M. He, C.-C. Su and Z. Zhang, The role of additives in improving performance in high voltage lithium-ion batteries with potentiostatic holds, *J. Electrochem. Soc.*, 2017, **164**, A6366, DOI: **10.1149/2.0471701jes**.

60 C. Han, Y.-B. He, M. Liu, B. Li, Q.-H. Yang, C.-P. Wong and F. Kang, A review of gassing behavior in $Li_4Ti_5O_{12}$-based lithium ion batteries, *J. Mater. Chem. A*, 2017, **5**, 6368–6381, DOI: **10.1039/C7TA00303J**.

61 Y.-B. He, B. Li, M. Liu, C. Zhang, W. Lv, C. Yang, J. Li, H. Du, B. Zhang, Q.-H. Yang, *et al.*). Gassing in $Li_4Ti_5O_{12}$-based batteries and its remedy, *Sci. Rep.*, 2012, **2**, 913, DOI: **10.1038/srep00913**.

62 R. Bernhard, S. Meini and H. A. Gasteiger, On-line electrochemical mass spectrometry investigations on the gassing behavior of $Li_4Ti_5O_{12}$ electrodes and its origins, *J. Electrochem. Soc.*, 2014, **161**, A497, DOI: **10.1149/2.013404jes**.